PCCP

PAPER

View Article Online
View Journal | View Issue

Cite this: *Phys. Chem. Chem. Phys.*, 2022, **24**, 28554

Systematic *in situ* hydration neutron reflectometry study on Nafion thin films†

Hamish Cavaye,[a] Rebecca J. L. Welbourn,[a] Jan G. Gluschke,[b] Paul Hughes,[c] Ky V. Nguyen,[b] Adam P. Micolich,[b] Paul Meredith[de] and A. Bernardus Mostert*[f]

Received 6th July 2022,
Accepted 7th November 2022

DOI: 10.1039/d2cp03067e

rsc.li/pccp

Reported herein is a neutron reflectometry (NR) study on hydrated Nafion thin films (~30 nm) on a silicon substrate with native oxide. The Nafion morphology is investigated systematically across the whole relative humidity range using both H_2O and D_2O vapours to enable a comparative study. By utilising this systematic approach two key results have been obtained. The first is that by leveraging the strong positive scattering signal from the D_2O vapour, a complete and systematic water adsorption isotherm (Type II) for a Nafion thin film is produced. Utilising the slight negative scattering signal of the H_2O enabled the quantification of the hydration dependent evolution of the formation of Nafion/water lamellae near the substrate surface. The number of lamellae layers increases continuously with hydration, and does not form abruptly. We also report the effects of swelling on the thin films across the relative humidity ranges. The work reported should prove useful in quantifying other hydration dependent properties of Nafion thin films such as conductivity and understanding Nafion/semiconductor based devices, as well as showcasing a NR methodology for other hydrophilic polymers.

Introduction

Nafion is a sulfonated fluoropolymer invented by the DuPont company and is famous for being a highly conductive proton ionomer (Fig. 1).[1,2] Due to its high proton conductivity and stability, Nafion has become a go-to solid-state soft electrolyte for a range of electrochemical devices including chemical sensors,[3–7] membrane fuel cells,[8–15] batteries[16–19] and water electrolyzers.[20–23] Nafion can be purchased as membranes, or can be bought as a solution from which thin films can be coated on a particular substrate. The thin film morphology (~5–500 nm thickness per Kusoglu & Weber)[2] has seen an increase in importance in recent years, especially for their potential roles as electrodes.[2] As such, a lot of research has been expended on understanding thin film morphological behaviour and their interaction with water.[24–29] However, the thin film morphology is not as well understood as the usual bulk membrane system,[2] and as such is the motivation for this work.

Some of the most comprehensive and insightful morphological work to date on thin films has been obtained using Neutron Reflectometry (NR), which gives atomic information throughout the thickness of a thin film.[27–29] In these previous NR studies, hydration effects were explored and comparisons made to water adsorption isotherms, *i.e.* quantification of water content as a function of relative humidity.[27] Work by Dura *et al.* for example,[27] also determined that a water/polymer lamellae phase forms near a SiO_2 substrate surface (a common device substrate) for a spin

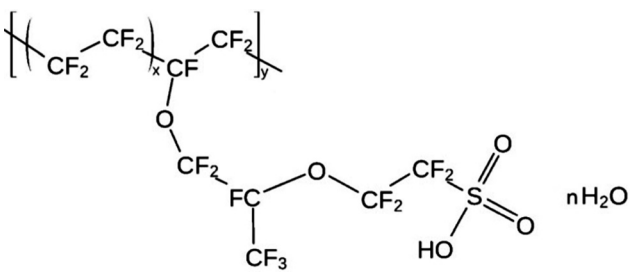

Fig. 1 The chemical structure of Nafion, with associated water molecules when hydrated. For Nafion 117 (the polymer employed in this work), the value of *x* would be approximately 6–7, such that one has around 14 CF_2 groups before a sulfonated pendant.[1]

[a] *ISIS Neutron and Muon Source, Rutherford Appleton Laboratory, Science and Technology Facilities Council, Didcot, OX11 0QX, UK*
[b] *School of Physics, University of New South Wales, Sydney, NSW 2052, Australia*
[c] *Centre for Nano Health, College of Engineering, Swansea University, Swansea SA2 8PP, UK*
[d] *Department of Physics, Swansea University, Singleton Park, SA2 8PP, Wales, UK*
[e] *School of Mathematics and Physics, University of Queensland, St Lucia Campus, Brisbane Queensland 4072, Australia*
[f] *Department of Chemistry, Swansea University, Singleton Park, Swansea, SA2 8PP, UK. E-mail: a.b.mostert@swansea.ac.uk*

† Electronic supplementary information (ESI) available. See DOI: https://doi.org/10.1039/d2cp03067e

coated Nafion thin film when hydrated. Additional work further refined and explored a wide range of film thicknesses from <12 nm[28] (or <120 Å) out to ~ 155 nm.[29] Yet there is currently no systematic, finely graded, hydration dependent NR work utilising either H_2O or D_2O on Nafion thin films. Especially utilising parallel setups on the same instrument to enable an enhanced and direct comparative study. As will be shown below, by utilising both H_2O and D_2O in a finely graded NR experiment, additional insights hereto not reported have been obtained. In particular, the H_2O based work gives insight into how the lamellae morphology near a substrate evolves as a function of hydration. Whereas the D_2O is more suited for bulk polymer/water morphology, enabling us to report the first complete water adsorption isotherm for a Nafion thin film morphology, which is a necessary data set for understanding Nafion thin film water interactions.

The work presented herein has specific implications for a recent innovation in Nafion processing. We recently demonstrated that by doing direct electron-beam exposure, Nafion 117 can be used as a negative electron beam lithography (EBL)-resist.[30] The material can then be patterned as a solid-state ionic electrolyte onto semiconductor nanowires to create ion-to-electron transducing transistors and inverters. These latter devices are able to transform or transduce an ionic signal into an electronic signal. The devices exhibited some of the best performance metrics (*e.g.* DC gain and switching speed) of current bioelectronic ionic-to-electronic transducing devices.[30] Critically, the performance of these Nafion-nanowire devices can be changed using hydration. Consequently, knowledge of the water distribution throughout the Nafion film as a function of hydration, near the semiconductor interface as well as the bulk, is of prime importance to understand these devices in more detail.

With the NR technique and hydration dependent approach, we will show two key results. The first is a complete water adsorption isotherm for a Nafion thin film, utilising the strong scattering signal of D_2O as an aid. The second result is the first quantification of the evolution of Nafion/water lamellae structure as a function of hydration. We show that H_2O is the better vapour to use for detecting the lamellae structure and that the evolution of the number of layers is gradual with hydration.

Methods

Basic approach

In the work reported herein, we utilise NR as a means to directly and non-destructively study thin film structures, particularly how they evolve as a function of hydration. In an NR experiment, neutrons are directed onto a thin film sample at a shallow angle and are reflected or refracted depending on the depth dependent composition of the film. The reflected neutron waves from each layer undergo interference, which leads to Kiessig fringes in the reflectivity as a function of the specular momentum transfer Q_z. The momentum transfer is the change of momentum of the reflected neutron perpendicular to the reflecting plane. This NR wave behaviour is dependent on both the incident angle θ and the neutron wavelength λ_{neutron}. So, the neutron wave's specular reflectivity momentum transfer can be expressed as:

$$Q_z = \frac{4\pi \sin\theta}{\lambda_{\text{neutron}}} \quad (1)$$

The spacing between the fringes is directly related to the thickness of any layers present within a film and the amplitude governed by the differences in neutron scattering length density or SLD:

$$\rho_i = \frac{\rho_{M,i} N_{\text{Av}}}{M_i} \sum_j n_j b_j \equiv \frac{1}{V_i} \sum_j n_j b_j \quad (2)$$

where $\rho_{M,i}$ is the mass density of species i, N_{Av} is Avogadro's number, M_i is the formula mass of species i, V_i is the molecular volume of species i, n_j is the number of atoms j in the molecular formula of species i, and b_j are their corresponding bound coherent neutron scattering lengths.[31] If a thin film, such as Nafion, is exposed to an environmental change such as a change in the humidity, this will lead to the sorption of vapour into the polymer structure, adding additional atomic species as a function of depth. As an illustration pertinent to the current experiment, if Nafion is exposed to H_2O or D_2O (heavy water) vapour the contrast in neutron scattering lengths of hydrogen ($b_H = -3.74$ fm) and deuterium ($b_D = 6.67$ fm) nuclei mean their SLD profiles will be significantly different. This will yield different reflectometry profiles for the different isotopes and thus allow one to better "track" the location of water vapour throughout the polymer film.[32]

Sample fabrication

Prime grade Si wafers with native oxide were used as substrates (Pi-KEM, single side polish, ⟨111⟩, n-type (phosphorus) with resistivity = 0.01–0.1 Ω cm, 525 ± 25 μm thickness, 2'' diameter). These substrates were prepared by 5 min sonication in acetone, 5 min sonication in 2-propanol, a 2-propanol rinse and N_2 blow-dry. Nafion 117 (Sigma-Aldrich, 5wt% solution) was diluted 1 : 3 with ethanol, the resulting mixture shaken for 30 s and then sonicated (Elmasonic Type S120H) for 5 minutes. Solution was pipetted onto the substrate to cover the entire surface ($\sim$1 mL) and spin coated for 60 s at 3500 rpm with a ramp speed of 1000 rpm s^{-1}.

Ellipsometry

All samples were checked for appropriate thickness and homogeneity of the Nafion layer by using a J.A. Woollam M-2000 ellipsometer. Scans were performed in a 13-point grid to ensure consistency across the sample. The data was fitted to a model assuming a Si substrate with native oxide with a two-parameter Cauchy layer. Values obtained for the Cauchy layer were $A = 1.332 \pm 0.002$ and $B = 0.00306 \pm 0.00009$ (2 times standard error, $n = 9$). The values obtained were similar to other published results.[13]

Neutron reflectometry

The measurements were performed using the INTER time-of-flight neutron reflectometer[33] at the ISIS Neutron and Muon source (Chilton, Oxfordshire, UK).[34] We used a fixed resolution

of $\Delta Q/Q$ = 2%, a footprint of 40 × 30 mm to minimise film edge effects, and a cold neutron spectrum (0.17 nm < $\lambda_{neutron}$ < 1.7 nm). The samples were placed on an aluminium stand within a sealed polyacrylic chamber with sapphire windows cut to the *c*-axis, custom-built for use at INTER. Two chambers were used in parallel, one for the D_2O vapour experiment and the other for H_2O to allow for efficient time use and to mitigate cross-contamination. Each chamber was connected to a "static" vapour pressure system (ESI,† Scheme S1). Similar systems have been employed elsewhere,[35–37] but in brief, the vapour delivery system consisted of a bellows vacuum steel hose attached with a BOC-Edwards pressure gauge (GK series, 0–50 mbar) and a degassed, deionised vial of water (either D_2O or H_2O). The line in turn was connected to a vacuum pump. The vapour pressure above the sample was controlled by manual valves, with one key valve attached to the vacuum pump (Valve 4, Scheme S1, ESI†) and the other connected to the water vial (Valve 3, Scheme S1, ESI†). The entire system was left in a temperature-controlled room (T = 24.8 ± 0.2 °C). A Nafion film, whether set for D_2O or H_2O exposure, was initially placed under vacuum (<0.01 mbar, Pirani gauge) and its reflectivity profile was recorded ("dry" state). Samples were then exposed to the desired pressure of H_2O or D_2O vapour and the reflectivity profile recorded. The sample chambers were then evacuated to purge the atmosphere and observe the reversibility of the sorption process before the next exposure to H_2O or D_2O. After changing the pressure within the chamber, data were recorded at an incident angle of θ = 0.8°. We observed at this angle that the time-resolved measurements showed equilibrium was reached in the film in under 10 minutes, though we waited an additional 3–4 hours before taking a measurement in full. The reflectivity profile was then recorded across the entire Q-range [0.008, 0.235]/Å^{-1} (θ = 0.5° and 2.0°) and normalised to direct beam profiles recorded for each sample chamber. We note that all data was obtained using "event mode", which allows for arbitrary time-slicing of the dataset during analysis. Though, we utilised only 1 time bin where we did not see any changes with time. Films were exposed to approximately 0%, 10%, 20%, 40%, 60%, 70%, 80% and 100% of the saturation pressures of H_2O and D_2O, which were measured to be 29.5 ± 0.3 mbar and 25.7 ± 0.2 mbar respectively. We note that the uncertainties are due to the pressure gauge, however, given the nature of the setup being at thermal equilibrium everywhere with an open water source the state of the system is at saturation, *i.e.* 100% relative humidity. In addition, no vapour condensation was observed on any part of the equipment, likely due to the fact that there were no temperature gradients across the equipment *vis-à-vis* the water vapour. It is important to note that the different absolute vapour pressures for H_2O and D_2O corresponding to each relative humidity (RH) value (% of saturation pressure) result from the different saturation pressures of H_2O and D_2O and not from a change in temperature. Furthermore, the absolute pressure measured for each data point changed during the experiment due to various factors such as outgassing/small temperature fluctuations. As such, the pressure values were taken as the mean between the initial and final measured pressures. The uncertainty was taken as the range and is shown in the adsorption isotherms.

Neutron reflectometry modelling

The reflectometry analysis was done using RASCAL (ISIS) in Matlab 2020a to obtain fits to the data.[38] The basic approach was to obtain a model fit based upon the least number of fitting parameters that still enabled an essential understanding of the film/water behaviour. Each distinct sample layer is described by a thickness, SLD (composition) and roughness using a Nevot-Croce approximation.[39]

For the data obtained using D_2O vapour, all hydration points could be simultaneously fitted using a single "multi-contrast" model to improve confidence in the result. The parameters for the Si native oxide layer were common for all hydration values. For each hydration, the bulk Nafion layer could be modelled with a single layer of uniform SLD. A bootstrapping analysis of the fit parameters was performed using 250 iterations per dataset and fully randomised starting fit variables to extract uncertainties. Fig. S1–S3 and Table S1 (ESI†) show further details of the fitting parameters.

Even though an initial bulk layer could be modelled to the H_2O data set (ESI,† Fig. S4–S6 and Table S2), due to the presence of a high Q feature/peak (Q > 0.2 Å^{-1}) associated with the presence of a water/Nafion lamellae structure near the substrate interface (see Fig. 4a),[27] additional modelling was conducted. The lamellae structure is expected to be hydration dependent.[27] As such, the fit parameters for the native substrate oxide layer were determined using the lowest hydration points, *i.e.*, those with the simplest models, and then fixed in the subsequent datasets at higher hydration exposure. Fits that account for the lamellae structure have their fitting parameters shown in the ESI,† Fig. S7–S9 and Table S3.

From the NR fits, two useful parameters derived from the hydroscopic property of Nafion are calculated. The first parameter is water uptake, which is defined as the number of water molecules per acid group in the ionomer film, λ, in line with previously published isotherm work on Nafion.[27,40–44] The change in water uptake from the dry film, $\Delta\lambda$ was obtained via:

$$\Delta\lambda = \frac{\sum_n b_n}{\sum_w b_w}\left(\frac{\int \mathrm{SLD_{RH}}}{\int \mathrm{SLD_{RH=0}}} - 1\right) \quad (3)$$

where $\sum_n b_n$ is the sum of the bound coherent neutron scattering lengths for all atomic nuclei present within Nafion in one repeat unit of the ionomer, $\sum_w b_w$ is the sum of the bound coherent neutron scattering lengths for the atomic nuclei within water, $\mathrm{SLD_{RH}}$ is the SLD profile of the film at a particular relative humidity/relative pressure (SLD as a function of thickness), $\mathrm{SLD_{RH=0}}$ is the SLD profile of the film under active vacuum conditions (SLD as a function of thickness for the dry film) though we note that there may be trace amounts of water still present. However, the dry SLD (3.9–4.0 × 10^{-6} Å^{-2}) is commensurate with what is expected for Nafion (4.1–4.2 × 10^{-6} Å^{-2}). Consequently, we treat any trace amount of water as

unimportant in the results below. The integrals extend over the entire thickness of the Nafion layer and the above calculation assumes that there is no water uptake in the silicon native oxide layer or the silicon substrate.

The second parameter extracted from the data sets is swelling of the film, which was straightforward to obtain simply by determining the changes in the length/depth of the SLD profiles. Swelling entails a proportional change in the Nafion film thickness between the hydration point in question and the results obtained under vacuum.

Results and discussion

We approach the following section in three parts to enable a logical discussion of the results. Discussed first are the NR data for a Nafion film exposed to D_2O vapour. We will show that we are able to extract a complete water adsorption isotherm for a Nafion thin film, a first of its kind. However as will become clear, D_2O did not allow investigation of the more subtle morphological aspects of a hydrated Nafion thin film. As such, H_2O-based data will be then discussed. This will allow us to extend our analysis of hydrated Nafion thin films and for the first time show the evolution of Nafion/water lamellae structure as a function of hydration. We then end the section with final remarks to draw out the key points.

Using D_2O to obtain an accurate adsorption isotherm for Nafion films

The NR profiles as a function of D_2O hydration alongside the corresponding best-fit model SLD profiles are shown in Fig. 2a. There is no sign of a high Q feature, unlike with the use of H_2O (see Fig. 4a and elsewhere).[27–29] Hence, the model employed used a single layer for the Nafion film, with the resultant SLD profiles, are depicted in Fig. 2b.

The SLD profile for the evacuated or dry Nafion film indicates a film thickness of 321 Å with a uniform SLD of 3.98×10^{-6} Å^{-2}, which corresponds to an approximate solid mass density of 1.89 g cm^{-3}. This Nafion film then undergoes the expected gradual increases in both film thickness and SLD as the level of D_2O hydration increases, due to swelling induced by increasing absorbed D_2O in the film and D_2O's large, positive scattering length density. We note that the modelling indicates that the SLD increase is uniform across the entire depth of the film, which suggests a homogenous distribution of D_2O throughout the film. At 100% RH the film thickness reached 381 Å, having swelled by approximately 20%. Use of additional layers in the models were tested, however, they did not provide statistically significant improvements on the fits.

The SLD profiles in Fig. 2b were used to extract an adsorption isotherm of water uptake value (λ_{D_2O}) using eqn (3), where we assume λ_{D_2O} = 0 at RH = 0%. This adsorption isotherm is displayed in Fig. 3a with the total water uptake estimated to be just over 6 D_2O molecules per acid site at 100% RH. Fig. 3a has the shape of a Type II isotherm,[45] with the data consistent with a sharp increase in water uptake at low RH, which slows and then increases greatly again at high RH. This behaviour is indicative of multilayer physisorption of an adsorbate on an adsorbent.[45] A third order polynomial was fitted to the data as a guide to the eye. This first, complete water adsorption isotherm for a Nafion thin film is well-defined due to the large, positive coherent scattering length of deuterium and in turn large SLD for D_2O. Hence, Fig. 3a shows that using D_2O and its strong signal is an excellent substitute for H_2O in extracting the total water content.

However, the positive SLD of D_2O does have a drawback here. Like other D_2O based work on comparable film thicknesses,[26] no high Q peak is seen in Fig. 2a, whereas a broad peak can be observed ($\sim$0.2 Å^{-1}) when Nafion is hydrated with H_2O.[27–29,46] The lack of peak in D_2O results is due to insufficient contrast between Nafion rich and D_2O rich regions. The negative scattering length density of H_2O though affords the necessary contrast (see Fig. 4a below for example).

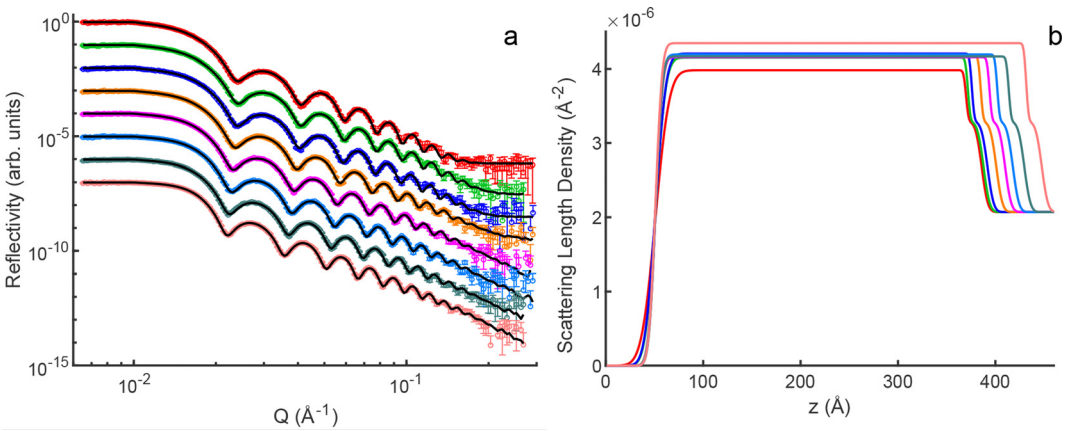

Fig. 2 (a) Neutron reflectometry profiles obtained at different D_2O vapour values (offset for clarity) with the modelling depicted as solid black lines. From top to bottom RH = 0, 9, 21, 40, 60, 72, 86, and 100%. (b) The corresponding, best fit SLD profiles obtained from the modelling. The line colours correspond to the respective profiles in (a). Low z (film thickness/depth) corresponds to the interface with air and high z corresponds to the bulk Si substrate.

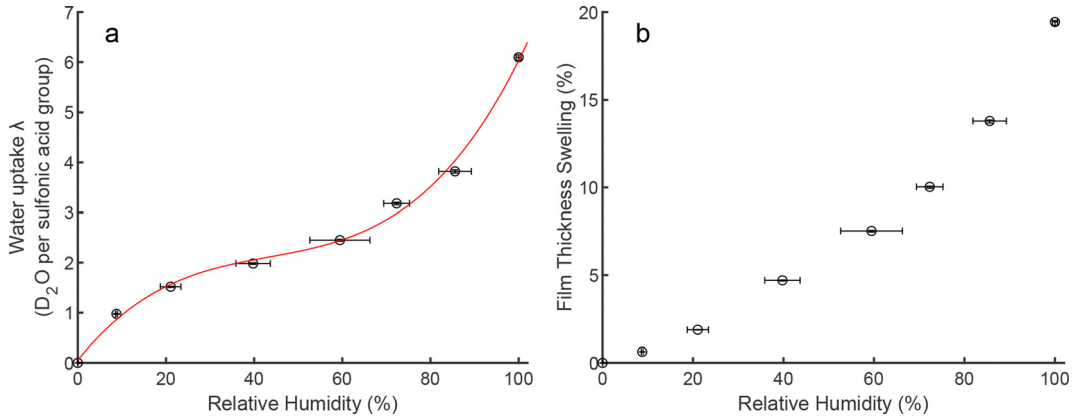

Fig. 3 (a) Change in water uptake *vs.* D_2O vapour RH (circles) with a 3rd order polynomial fit to the isotherm data (solid line). (b) Film thickness swelling percentage *vs.* D_2O relative humidity.

As a cross check, our adsorption result in Fig. 3a is checked for consistency with other NR work. All the work cited below do not produce a complete isotherm as we do here, but they do report λ values at very high RH, in the range of 92–100%, which we can compare with our own result at 100% RH ($\lambda \sim 6.2$ using D_2O). In DeCaluwe *et al.* the authors did a systematic study of Nafion thin films with varying thickness.[29] Using their data (see ESI†) and linear interpolation, we estimate that for a thickness of Nafion film corresponding to our own, one would obtain a value of $\lambda \sim 6.3$, which is close to the $\sim$6.2 obtained for the D_2O isotherm in this study. Dura *et al.* in their study reported a film of a thickness and substrate closest to our own, 42 nm thick film, had a λ value of $\sim$5.[27] Finally, Kalisvaart *et al.* reported a value of $\sim$6.9 on a 15 nm thick film utilising D_2O, before a heating cycle on the film, which subsequently yielded $\sim$9.1.[26] Overall, our high humidity result is consistent with the reported literature.

Additional data can be extracted from Fig. 2b such as film swelling in Fig. 3b. Fig. 3b shows the film swelling for each hydration point, with the thickness swelling appearing to be roughly quadratic across the full hydration range. Fig. 3b should prove useful for, *e.g.*, calibrating accurate conductivity values of Nafion thin films as a function of hydration, measurements that are of keen interest.[24,29,30] When Fig. 3a and b are taken together, the adsorption and thickness changes do not show the same qualitative behaviour, with the swelling slower to increase with relative humidity. This observation can be interpreted as the initial water uptake occurring at high-affinity, easy-access sites, which produce little swelling of the film. As the humidity increases and water multilayering occurs, a more pronounced change in film thickness is then produced, *i.e.* production of water-rich regions.

Overall, in this section, we report the first, complete water adsorption isotherm for a Nafion thin film morphology as depicted in Fig. 3a.

Using H_2O to probe Nafion/water lamellae morphology

An equivalent hydration experiment to the D_2O one was performed using H_2O as the adsorbate. The NR measurements on

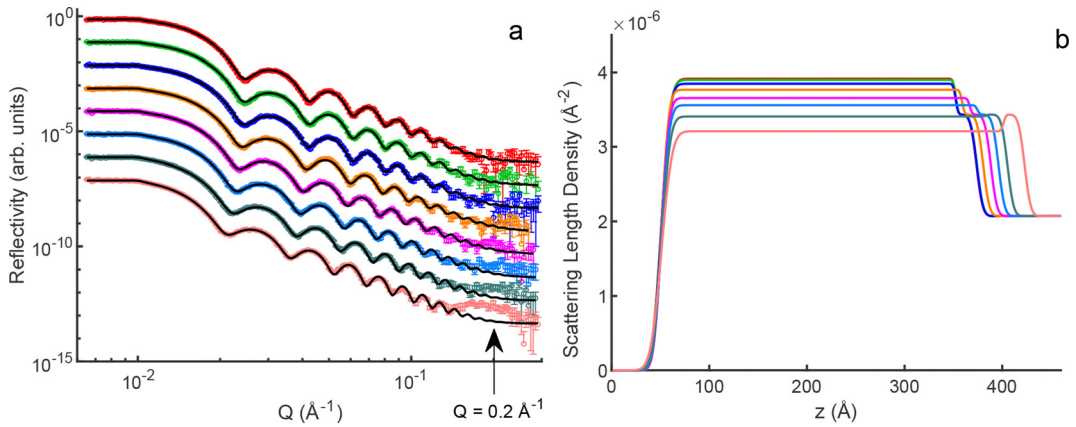

Fig. 4 (a) Neutron reflectometry profiles obtained at different H_2O vapour values (offset for clarity) with the modelling of a single uniform Nafion layer depicted as a solid black line. From top to bottom the RH were: 0, 8, 22, 35, 56, 69, 80, and 100%. The arrow with corresponding *Q* value indicates the emergence of a feature seen for highly hydrated films. (b) The corresponding, best fit SLD profiles obtained from the modelling using just a single uniform Nafion layer. The line colours correspond to the respective profiles in (a). Low *z* corresponds to the interface with air and high *z* corresponds to the bulk Si substrate.

the evacuated Nafion film used for the H_2O experiment revealed a dry film thickness of 301 Å. Hence the data should be directly comparable to the films exposed to D_2O.

Fig. 4a shows the NR data for the H_2O hydration experiment alongside a set of fits using the same type of model as for the D_2O data, *i.e.* using a single homogeneous layer to represent the Nafion layer, where the number of fit parameters is minimised. Fig. 4b shows the corresponding SLD profiles for these fits. At low RH (0%, 8%, and 22%) the data are sufficiently described by this single layer fit. However, as the RH increases a feature/peak at high Q ($\sim$0.2 Å^{-1}) becomes apparent that is not accounted for using the model. Nonetheless, given the good fit to the fringe structure at lower Q values, the general SLD trend provides a strong indication of the overall layer behaviour: an expected trend of film swelling in agreement with the D_2O data, and overall decrease in SLD due to the negative SLD of the H_2O within the film.

The high Q feature observed is a reported feature in other NR work on Nafion,[27–29] which is ascribed to a lamellar structure forming at the Nafion-substrate interface.[27–29] The lamellar structure is formed by sequential layers of water rich and Nafion rich regions.[27–29] With this literature in mind, we modified the modelling for the data depicted in Fig. 4a to include a lamellar structure, which is discussed in detail in the methods section. Fig. 5 shows the results of this new modified model compared to the data. Fig. 5 shows that the model now replicates (especially at high hydration), the peak at high Q. Fig. 6 shows the corresponding SLD profiles for the more complex models, where each profile is plotted separately for clarity. In Fig. 6, each hydration dependent SLD curve depicted was found to be the simplest model that provided significant improvements to fitting the data *vs.* using single layer models. Any additional lamellae were found to be unnecessary at the resolution of the experiment performed in this study.

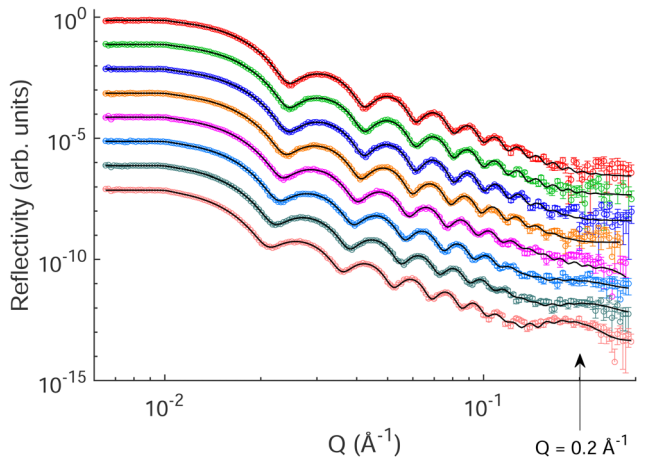

Fig. 5 Neutron reflectometry profiles obtained at different H_2O vapour values (offset for clarity) with the lamellar modelling depicted as a solid black line. From top to bottom the RH were: 0, 8, 22, 35, 56, 69, 80, and 100%. The arrow with corresponding Q value indicates the emergence of a feature seen for highly hydrated films.

These experiments are consistent with the lamellar structure being at the Nafion/substrate interface. However, they do not preclude the lamellae being elsewhere in the film, *e.g.* at the air/Nafion interface. Currently, we have accepted the models of the prior literature since there are no clear contradictions with previous work, but we do not claim the models used here are the only possible solutions to fit the data.

By interrogating each hydration point individually it was possible to begin to investigate the evolution of the formation of lamellae as a function of hydration, which to date has not been done to this fine a gradation in hydration. At very low hydration levels (RH = 0% & 8%, Fig. 6a and b) the data are well described without the need for any additional layers. At RH = 22% and 35% (Fig. 6c and d) there is one additional thin layer of increased SLD at the substrate, *i.e.*, a very thin Nafion rich layer. The number of required lamellae increases to two, one H_2O rich layer (SLD dip) and one Nafion rich layer (SLD peak) at RH = 56% (Fig. 6e). There are then three lamellae at RH = 69% (Fig. 6f) alternating from the substrate between H_2O, Nafion, H_2O rich layers. Lastly, at the highest levels of hydration (RH = 80% and 100%) there is a total of four lamellae (Fig. 6g and h), starting with a H_2O rich layer near the substrate. Importantly, we emphasise that this does not indicate a precise determination of the number of lamellae in each structure due to the technique resolution, diffraction limit and being a single contrast fit (*i.e.*, level of information present). However, it does show clear evidence for a trend of steadily increasing multilayers as RH increases and not some critical hydration at which these structures spontaneously form. The thickness of the lamellae also increases slightly with hydration (5 Å at 22% RH and 11–14 Å at 100% RH). This is also consistent with the swelling being primarily driven by the gradual formation of water-rich regions, as outlined by the relative shapes in Fig. 3.

Our experiments were done on a single, spin coated Nafion thin film on a Si substrate with oxide surface. This is similar to DeCaluwe *et al.*'s work, where they made an observation that under vacuum there are three lamellae. These lamellae are due to alternating regions of higher/lower density of Nafion *vs.* the rest of the bulk, and presumably is the origin for water able to penetrate and fill the lower density areas.[27–29] In principle, we could also apply a lamellar model to the dry state, but believe this would stretch the information content of the data presented here and instead choose to reduce ambiguity with a single layer for the Nafion film. A higher resolution technique such as GIXD is better placed to determine any finer details. When hydrated to very high relative humidity, DeCaluwe *et al.* reported 6 lamellae structures for similar thickness of film (their 70 Å–600 Å range).[29] This is consistent with the appearance of lamellar structures on increasing RH found in this work. Overall, our data does not show significant evidence for lamellae at low RH values, though this is not discounted, but it does show strong evidence that they are more pronounced at high RH values, *i.e.* that there is a continuum of lamellae structure formation.

Utilising the lamellae modelling, we then interrogated the water content and film thicknesses in the same manner as the

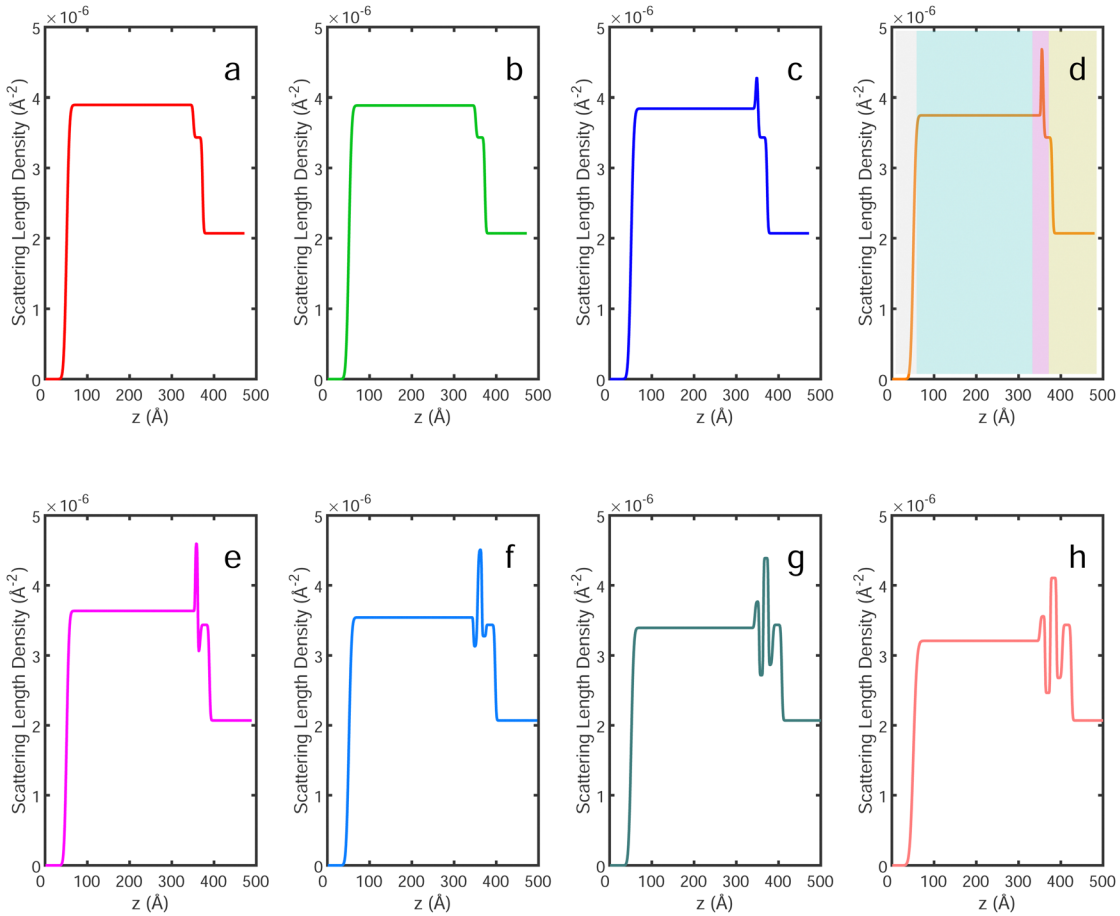

Fig. 6 The corresponding SLD profiles to Fig. 5 obtained from the modelling, which include accounting for the lamellae. These have been plotted separately for clarity. The RH for each dataset were: (a) 0%, (b) 8%, (c) 22%, (d) 35%, (e) 56%, (f) 69%, (g) 80%, and (h) 100%. To aid in understanding the assignment of the various layers, figure (d) has been shaded. The various areas indicate various regions, yellow indicates the substrate, pink the lamellae region, light blue the bulk and grey the environment/air.

D_2O hydration data (Fig. 7, compared with Fig. 3). An adsorption isotherm for the H_2O data is depicted in Fig. 7a, with the corresponding D_2O isotherm in Fig. 3a. The overall water adsorption at high RH values is comparable to the D_2O data, with λ_{H_2O} being approximately 7 at 100% RH (*cf.* approximately 6 for D_2O). Unlike the D_2O isotherm, the H_2O plot exhibits a greater scatter. We ascribe this scatter to the relative SLDs of D_2O > Nafion > H_2O, and the subsequent effect on the λ calculation. When D_2O is absorbed by the Nafion film, the combination of film swelling and increase in film SLD leads to

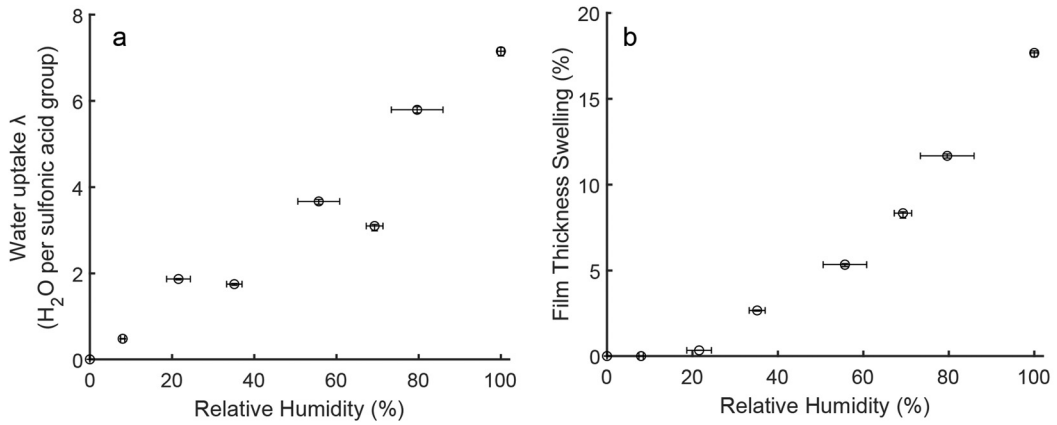

Fig. 7 (a) Change in water uptake *vs.* H_2O vapour RH (circles). (b) Film thickness swelling percentage *vs.* H_2O vapour RH.

a large increase in the difference in integrated area under the SLD profiles, which is used to calculate water uptake. For H_2O, however, while the film swells, the overall SLD of the film is reduced by the negative scattering length of the hydrogen atoms in the H_2O. These two factors lead to a cancelling effect in the integrated area of the SLD profiles. In turn this leads to smaller changes in integrated areas between hydration points, and thus to a greater uncertainty in λ. This particular uncertainty could not be accurately quantified in our analysis and so is not represented in the *y*-axis error bars in the plot, but is likely to be the main source of the increased scatter in Fig. 7a. Due to this increased scatter we did not attempt to fit a polynomial to the H_2O isotherm data. Consequently, we are unable to make a definite statement regarding the type of isotherm and the resulting adsorption mechanism. But our data indicate that there is no significant difference in overall water uptake between D_2O and H_2O for a Nafion film of this thickness. As such, the H_2O data set appears to be consistent with the D_2O result in Fig. 3a. And, as will be discussed below regarding swelling behaviour, the activity (relative humidity) is the determinative factor in the equilibrium film behaviour. Hence, the D_2O isotherm should be a direct indication of H_2O behaviour.

Film thickness swelling was found to be very similar for H_2O and D_2O (Fig. 7b), with the film swelling in an approximately quadratic way as a function of hydration, from 301 Å at 0% RH up to 353 Å at 100% RH, *i.e.* approximately 18% thickness swelling. This almost identical result to the D_2O data is a more significant observation than may be first realised. To understand this point, one has to keep in mind that H_2O and D_2O vapour have quite different saturation pressures ($\sim$20% difference at room temperature). As such, a question to ask is whether the water dependent morphological properties of the Nafion are going to depend on the absolute pressure of the vapour, or the activity of the water in the film (as measured by the relative humidity at equilibrium). This can be important in understanding the adsorption mechanism, *e.g.* different adsorption isotherms can either have a relative humidity or absolute pressure dependence.[45] Inspecting Fig. S11 (ESI†), one can see that the two curves are offset when plotted against absolute pressure, particularly noticeable at the high pressure values. Instead, the curves align on top of one another when plotted *vs.* relative humidity. Given this latter result, it would indicate that the behaviour of both films are commonly described by the activity (relative humidity), and thus is the appropriate normalisation for comparison.

Final remarks

Overall, we showed that understanding Nafion thin film morphological behaviour as pertaining to its hydration response requires a systematic approach. As this study specifically highlights, absent from previous work, a systematic approach especially requires the use of both D_2O and H_2O for NR studies, since both vapours have their own strengths and weaknesses.

D_2O as the adsorbate enabled the extraction of a complete, water adsorption isotherm that is depicted in Fig. 3a. This is due to D_2O having a large positive SLD that produces a clear trend, commensurate with the effect of swelling on the SLD profile. In short, a novel insight of this work is that the D_2O is an excellent vapour to use on Nafion thin films to probe 1st order morphological effects, *i.e.* the bulk effects.

In contrast, the H_2O as an adsorbate, due to its slight negative SLD, makes the extraction of the H_2O content in a hydrated Nafion SLD difficult. Hence, it is not as optimal for bulk effects as the D_2O. However, precisely due to the greater contrast with Nafion, the H_2O data can be used to extract more subtle, 2nd order morphological effects. Specifically, for Nafion thin films, the subtle features in the reflectometry profiles could be enhanced compared to D_2O measurements alone. This, coupled with the systematic hydration approach, have allowed us to quantify for the first time the evolution of Nafion/water lamellae near a substrate surface with hydration.

We note, that unlike previous works, our work can distinguish between a continuous evolution of lamellae fomration with hydration *versus* a phase like transition at a critical water content. Our data as depicted in Fig. 6 supports a continuous evolution view.

As such, we believe the methodology shown above, systematic hydration control using both H_2O and D_2O vapours is a powerful approach to polymer systems for future NR work.

Conclusions

In conclusion, we have performed an *in situ* hydration study on Nafion thin films ($\sim$30 nm) using new experimental hardware for NR measurements at the ISIS facility. These new procedures included a parallel setup utilising D_2O and H_2O adsorption separately, employing multiple hydration points for each vapour to map out complete water adsorption isotherms.

The first key result is a complete water adsorption isotherm that was obtained using D_2O vapour, but which should be directly applicable to understanding H_2O vapour uptake.

The second key result is the first systematic quantification of Nafion/water lamellae structures as a function of hydration, which was enabled by using H_2O. The results show that the water/Nafion lamellae structures gradually develop with increasing hydration and do not undergo a distinct change at a particular hydration level.

The work presented here should prove useful in understanding new Nafion/semiconductor based devices whose performance is based upon hydration, calibrating the conductive properties of Nafion thin films and furthering the NR technique for hydrophilic polymers.

Author contributions

Sample preparation was done by A. B. M., K. N. and J. G. G. NR data was collected by H. C., R. W., J. G. G., P. H. and A. B. M. Ellipsometry data was obtained by A. B. M. and K. N. The NR data was analysed by H. C. and R. W. Design of the experiment was performed by A. B. M., P. H., H. C. and R. W. Original

conception of the work was by A. B. M., P. M. and A. P. M. Project was managed by A. B. M. Initial draft written by A. B. M., H. C. and R. W. All authors contributed to the final manuscript.

Conflicts of interest

There are no conflicts of interest to declare.

Acknowledgements

This work was funded by the Australian Research Council (ARC) under DP170104024 and DP170102552, the Welsh European Funding Office (European Regional Development Fund) through the Sêr Cymru II Program. P. M. is a Sêr Cymru II National Research Chair, which is supported by the Welsh Government through the European Regional Development Fund and an Honorary Professor at the University of Queensland. A. B. M. is a Sêr Cymru II fellow and the results incorporated in this work is supported by the Welsh Government through the European Union's Horizon 2020 research and innovation program under the Marie Skłodowska-Curie grant agreement No 663830. P. H. is funded by the Welsh Government's Sêr Cymru II Program through the European Regional Development Fund, Welsh European Funding Office, and Swansea University Strategic Initiative in Sustainable Advanced Materials. This work was performed in part using the NSW node of the Australian National Fabrication Facility (ANFF).

References

1 K. A. Mauritz and R. B. Moore, State of Understanding Nafion, *Chem. Rev.*, 2004, **104**, 4535–4585.
2 A. Kusoglu and A. Z. Weber, New Insights into Perfluorinated Sulfonic-Acid Ionomers, *Chem. Rev.*, 2017, **117**(3), 987–1104.
3 S. M. Ayyadurai, A. D. Worrall, J. A. Bernstein and A. P. Angelopoulos, Perfluorosulfonic Acid Membrane Catalysts for Optical Sensing of Anhydrides in the Gas Phase, *Anal. Chem.*, 2010, **82**(14), 6265–6272.
4 K. A. Frith and J. L. Limson, Reprint of ''pH tuning of Nafion® for selective detection of tryptophan'', *Electrochim. Acta*, 2010, **55**(14), 4281–4286.
5 Y. Lin, Q. Zhou, Y. Lin, D. Tang, G. Chen and D. Tang, Simple and sensitive detection of aflatoxin B1 within five minute using a non-conventional competitive immunosensing mode, *Biosens. Bioelectron.*, 2015, **74**, 680–686.
6 M. Shariatgorji, J. Astorga-Wells and L. L. Ilag, Trends in the bioanalytical applications of microfluidic electrocapture, *Anal. Bioanal. Chem.*, 2011, **399**(1), 191–195.
7 J. Zavazalova, M. E. Ghica, K. Schwarzova-Peckova, J. Barek and C. M. A. Brett, Carbon-Based Electrodes for Sensitive Electroanalytical Determination of Aminonaphthalenes, *Electroanalysis*, 2015, **27**(7), 1556–1564.
8 A. Kusoglu, A. Kwong, K. T. Clark, H. P. Gunterman and A. Z. Weber, Water Uptake of Fuel-Cell Catalyst Layers, *J. Electrochem. Soc.*, 2012, **159**(9), F530–F535.
9 B. Kientiz, H. Yamada, N. Nonoyama and A. Z. Weber, Interfacial Water Transport Effects in Proton-Exchange Membranes, *J. Fuel Cell Sci. Technol.*, 2010, **8**, 1.
10 J. D. Fairweather, D. Spernjak, A. Z. Weber, D. Harvey, S. Wessel, D. S. Hussey, D. L. Jacobson, K. Artyushkova, R. Mukundan and R. L. Borup, Effects of Cathode Corrosion on Through-Plane Water Transport in Proton Exchange Membrane Fuel Cells, *J. Electrochem. Soc.*, 2013, **160**(9), F980–F993.
11 N. Nonoyama, S. Okazaki, A. Z. Weber, Y. Ikogi and T. Yoshida, Analysis of Oxygen-Transport Diffusion Resistance in Proton-Exchange-Membrane Fuel Cells, *J. Electrochem. Soc.*, 2011, **158**(4), B416.
12 D. K. Paul, A. Fraser and K. Karan, Towards the understanding of proton conduction mechanism in PEMFC catalyst layer: Conductivity of adsorbed Nafion films, *Electrochem. Commun.*, 2011, **13**(8), 774–777.
13 D. Paul, A. Fraser, J. Pearce and K. Karan, Understanding the Ionomer Structure and the Proton Conduction Mechanism in PEFC Catalyst Layer: Adsorbed Nafion on Model Substrate, *ECS Trans.*, 2011, **41**(1), 1393–1406.
14 M. Secanell, K. Karan, A. Suleman and N. Djilali, Multivariable optimization of PEMFC cathodes using an agglomerate model, *Electrochim. Acta*, 2007, **52**(22), 6318–6337.
15 A. Z. Weber and A. Kusoglu, Unexplained transport resistances for low-loaded fuel-cell catalyst layers, *J. Mater. Chem. A*, 2014, **2**(41), 17207–17211.
16 R. M. Darling, A. Z. Weber, M. C. Tucker and M. L. Perry, The Influence of Electric Field on Crossover in Redox-Flow Batteries, *J. Electrochem. Soc.*, 2015, **163**(1), A5014–A5022.
17 I. Bauer, S. Thieme, J. Brückner, H. Althues and S. Kaskel, Reduced polysulfide shuttle in lithium–sulfur batteries using Nafion-based separators, *J. Power Sources*, 2014, **251**, 417–422.
18 N. Wang, S. Peng, D. Lu, S. Liu, Y. Liu and K. Huang, Nafion/TiO2 hybrid membrane fabricated via hydrothermal method for vanadium redox battery, *J. Solid State Electrochem.*, 2012, **16**(4), 1577–1584.
19 X. Wu, J. Hu, J. Liu, Q. Zhou, W. Zhou, H. Li and Y. Wu, Ion exchange membranes for vanadium redox flow batteries, *Pure Appl. Chem.*, 2014, **86**(5), 633–649.
20 S. Kumari, Turner White, R. Kumar, B. Spurgeon and J. M. Solar, hydrogen production from seawater vapor electrolysis, *Energy Environ. Sci.*, 2016, **9**(5), 1725–1733.
21 P. Millet, R. Ngameni, S. A. Grigoriev, N. Mbemba, F. Brisset, A. Ranjbari and C. Etiévant, PEM water electrolyzers: From electrocatalysis to stack development, *Int. J. Hydrogen Energy*, 2010, **35**(10), 5043–5052.
22 C. Rozain and P. Millet, Electrochemical characterization of Polymer Electrolyte Membrane Water Electrolysis Cells, *Electrochim. Acta*, 2014, **131**, 160–167.
23 S. Siracusano, V. Baglio, N. Briguglio, G. Brunaccini, A. Di Blasi, A. Stassi, R. Ornelas, E. Trifoni, V. Antonucci and

A. S. Aricò, An electrochemical study of a PEM stack for water electrolysis, *Int. J. Hydrogen Energy*, 2012, **37**(2), 1939–1946.

24 M. A. Modestino, D. K. Paul, S. Dishari, S. A. Petrina, F. I. Allen, M. A. Hickner, K. Karan, R. A. Segalman and A. Z. Weber, Self-Assembly and Transport Limitations in Confined Nafion Films, *Macromolecules*, 2013, **46**, 867–873.

25 A. Kongkanand, Interfacial Water Transport Measurements in Nafion Thin Films Using a Quartz-Crystal Microbalance, *J. Phys. Chem. C*, 2011, **115**(22), 11318–11325.

26 W. P. Kalisvaart, H. Fritzsche and W. Mérida, Water Uptake and Swelling Hysteresis in a Nafion Thin Film Measured with Neutron Reflectometry, *Langmuir*, 2015, **31**(19), 5416–5422.

27 J. A. Dura, V. S. Murthi, M. Hartman, S. K. Satija and C. F. Majkrzak, Multilamellar Interface Structures in Nafion, *Macromolecules*, 2009, **42**, 4769–4774.

28 S. C. DeCaluwe, P. A. Kienzle, P. Bhargava, A. M. Baker and J. A. Dura, Phase segregation of sulfonate groups in Nafion interface lamellae, quantified via neutron reflectometry fitting techniques for multi-layered structures, *Soft Matter*, 2014, **10**(31), 5763–5776.

29 S. C. DeCaluwe, A. M. Baker, P. Bhargava, J. E. Fischer and J. A. Dura, Structure-property relationships at Nafion thin-film interfaces: Thickness effects on hydration and anisotropic ion transport, *Nano Energy*, 2018, **46**, 91–100.

30 J. G. Gluschke, J. Seidl, R. W. Lyttleton, K. Nguyen, M. Lagier, F. Meyer, P. Krogstrup, J. Nygård, S. Lehmann, A. B. Mostert, P. Meredith and A. P. Micolich, Integrated bioelectronic proton-gated logic elements utilizing nanoscale patterned Nafion, *Mater. Horiz.*, 2021, **8**, 224–233.

31 V. F. Sears, Neutron scattering lengths and cross sections, *J. Neutron Res.*, 1992, **3**, 26–37.

32 A. J. Clulow, A. B. Mostert, M. Sheliakina, A. Nelson, N. Booth, P. L. Burn, I. R. Gentle and P. Meredith, The structural impact of water sorption on device-quality melanin thin films, *Soft Matter*, 2017, **13**, 3954–3965.

33 A. B. Mostert, H. Cavaye, A. P. Micolich, R. Welbourn, P. Meredith, J. G. Gluschke and P. Hughes, *Water adsorption isotherms for Nafion*, ISIS Neutron and Muon Source, Chilton, Oxfordshire, UK, 2019, DOI: **10.5286/ISIS.E.RB1910351**.

34 ISIS Neutron and Muon Source, **https://www.isis.stfc.ac.uk/** (Accessed 2022 March 21).

35 A. B. Mostert, B. J. Powell, I. R. Gentle and P. Meredith, On the origin of electrical conductivity in the bio-electronic material melanin, *Appl. Phys. Lett.*, 2012, **100**, 093701.

36 A. B. Mostert, S. B. Rienecker, C. Noble, G. R. Hanson and P. Meredith, The photoreactive free radical in eumelanin, *Sci. Adv.*, 2018, **4**, eaaq1293.

37 A. B. Mostert, S. Rienecker, M. Sheliakina, P. Zierep, G. R. Hanson, J. R. Harmer, G. Schenk and P. Meredith, Engineering Proton Conductivity in Melanin Using Metal Doping, *J. Mater. Chem. B*, 2020, **8**, 8050–8060.

38 A. Hughes RASCAL, Beta 1; ISIS Neutron Source, Rutherford Appleton Laboratory.

39 R. Pynn, Neutron scattering by rough surfaces at grazing incidence, *Phys. Rev. B: Condens. Matter Mater. Phys.*, 1992, **45**(2), 602–612.

40 P. Choi, N. H. Jalani and R. Datta, Thermodynamics and Proton Transport in Nafion, *J. Electrochem. Soc.*, 2005, **152**(3), E84.

41 T. A. Zawodzinski, M. Neeman, L. O. Sillerud and S. Gottesfeld, Determination of Water Diffusion Coefficients in Perfluorosulfonate Ionomeric Membranes, *J. Phys. Chem.*, 1991, **95**, 6040–6044.

42 D. R. Morris and X. Sun, Water-sorption and Transport Properties of Nafion 117 H, *J. Appl. Polym. Sci.*, 1993, **50**, 1445–1452.

43 K. K. Pushpa, D. Nandan and R. M. Iyer, Thermodynamics of water sorption by perfluorosulphonate (Nafion-117) and polystyrene–divinylbenzene sulphonate (Dowex 50W) ion-exchange resins at 298 ± 1 K, *J. Chem. Soc., Faraday Trans. 1*, 1988, **84**(6), 2047–2056.

44 D. Rivin, C. E. Kendrick, P. W. Gibson and N. S. Schneider, Solubility and transport behavior of water and alcohols in Nafion™, *Polymer*, 2001, **42**(2), 623–635.

45 G. Barnes and I. Gentle, *Interfacial Science: An Introduction*, Oxford University Press, 2nd edn, 2011, p. 336.

46 S. A. Eastman, S. Kim, K. A. Page, B. W. Rowe, S. Kang, C. L. Soles and K. G. Yager, Effect of Confinement on Structure, Water Solubility, and Water Transport in Nafion Thin Films, *Macromolecules*, 2012, **45**(19), 7920–7930.